CrossMark

Experimental Study and Thermodynamic Re-optimization of the FeO-Fe$_2$O$_3$-SiO$_2$ System

Taufiq Hidayat[1] · Denis Shishin[1] · Sergei A. Decterov[2] · Evgueni Jak[1]

Abstract Phase equilibria and thermodynamic data in the FeO-Fe$_2$O$_3$-SiO$_2$ system were critically reviewed. New experiments were undertaken to resolve discrepancies found in previous data. The liquid oxide/slag phase was described using the modified quasichemical model. New optimized parameters of the thermodynamic models for the Gibbs energies of slag and other phases in the selected system were obtained. The new parameters reproduce all available phase equilibria and thermodynamic data within the experimental error limits from 298 K (25 °C) to above the liquidus temperatures at all compositions and oxygen partial pressures from metal saturation to 1 atm of O$_2$. This study was carried out as part of the development of a self-consistent thermodynamic database for the Al-Ca-Cu-Fe-Mg-Si-O-S multi-component system.

✉ Taufiq Hidayat
t.hidayat@uq.edu.au

1 Pyrometallurgy Innovation Centre, School of Chemical Engineering, The University of Queensland, Brisbane, QLD, Australia

2 Centre de Recherche en Calcul Thermochimique (CRCT), Dép. de Génie Chimique, École Polytechnique, Montreal, QC, Canada

1 Introduction

The FeO-Fe$_2$O$_3$-SiO$_2$ system is essential for most pyrometallurgical processes, as well as for many other fields, such as ceramics and petrology. The system describes the chemical basis for sintering of iron-containing ores, slags in steel making, and non-ferrous sulfide smelting. Accurate description of the phase equilibria and thermodynamic properties of the system over a wide range of conditions is required for calculations and simulations to assist in the evaluation of the performance of the industrial processes.

The FeO-Fe$_2$O$_3$-SiO$_2$ system has been extensively studied. Several researchers investigated the liquidus of the slag in equilibrium with metallic iron[1–4] and air,[5,6] and the miscibility gap of the slag at high temperatures.[7,8] Experimental data were reported by various researchers on the equilibria between gas and fully liquid slag;[6,9,10] between gas and two condensed phases (slag + solid iron, liquid iron, wüstite, magnetite, or tridymite);[1,3,6,10–17] and between gas and three condensed phases (three solids, or slag + two solids).[1,3,10,16,18–29] The experimental data were obtained using various experimental techniques including: (a) gas equilibration and quenching, followed by microstructural analysis, wet chemistry or EPMA;[1–8,10–13,15,17,20,23–25] and (b) gas equilibration and various types of online measurement, such as, thermogravimetric technique, e.m.f. technique with zirconia solid electrolytes or gas analysis technique.[9,16,18,19,21–23,26–29] The enthalpy of dissolution of solid SiO$_2$ in the FeO-Fe$_2$O$_3$ melt at 1693 K (1420 °C) was measured using a high-temperature calorimetry technique.[30,31]

There are several comprehensive assessments of the FeO-Fe$_2$O$_3$-SiO$_2$ system available in the literature. Goel et al.[32] modeled the system by considering Fe, FeO,

478

J. Phase Equilib. Diffus. (2017) 38:477–492

$FeO_{1.5}$ and SiO_2 species in the liquid phase. Bjorkman[33] described the slag phase as an ideal solution made up of FeO, $FeO_{1.5}$ and three iron–silicate complexes Fe_2SiO_4, $Fe_3Si_2O_7$ and $Fe_3Si_6O_{15}$. Wu et al.[34] described the FeO-SiO_2 slag using the quasichemical model. Selleby[35] and Fabrichnaya and Sundman[36] modelled the liquid phase in the Fe-O-Si system using the sublattice formalism. The liquid solution in these studies[35,36] covered wide range of compositions from liquid metal to molten oxide. The most recent work was carried out by Jak et al.[37] in which the slag was described by FeO, $FeO_{1.5}$ and SiO_2 components using a modified quasichemical model.

The phase diagram of the Fe-O-Si system at 1473 K (1200 °C) is shown in Fig. 1.[38] The present study focuses on the FeO-Fe_2O_3-SiO_2 part of the Fe-O-Si system. The FeO-Fe_2O_3-SiO_2 sub-system was previously assessed by Jak et al.[37] and has been re-optimized to provide better description of phase equilibria and thermodynamic data in the system and to incorporate new experimental data obtained in the present study.

A thermodynamic "optimization" of a system using the CALPHAD approach involves critical simultaneous evaluation of all available phase equilibria and thermodynamic data to obtain one set of model equations for the Gibbs energies of all phases as functions of temperature and composition.[39] The accuracy of the database can then be tested by back-calculating the thermodynamic properties and the phase diagrams from the model equations to ensure that all data have been reproduced within the experimental error limits. Thermodynamic property data, such as activity data, can aid in assessing the phase diagram and phase
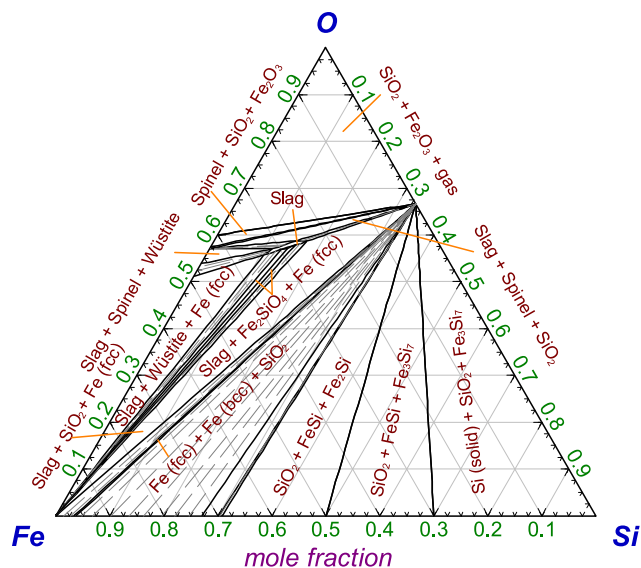
diagram measurements can be used to derive the thermodynamic properties. If discrepancy in the available data is found during the development of the model, new experimental measurements can be undertaken so as to provide the data essential for further refinement of the model equations. The present thermodynamic optimization was performed using FactSage thermodynamic software package[40] as part of the development of the self-consistent thermodynamic database for the Al-Ca-Cu-Fe-Mg-Si-O-S multi-component system.

2 Present Experimental Work

In most of non-ferrous smelting processes, the operational window for fayalite slags is typically limited by spinel and tridymite liquidi. Targeted experiments in the FeO-Fe_2O_3-SiO_2 system were carried out in the present study using equilibration/quenching/EPMA (Electron Probe x-ray Microanalysis) technique focusing on the slag, spinel and tridymite equilibrium at fixed oxygen partial pressures and at selected temperatures to resolve discrepancies found in previous data.[1,16,20]

Several sets of equilibration experiments at oxygen partial pressures of 0.21, 10^{-5}, 10^{-6} and 10^{-8} atm were conducted to determine temperature and slag composition at the equilibrium with spinel and tridymite in the FeO-Fe_2O_3-SiO_2 system by systematic variation of CaO concentration followed by the extrapolation from the CaO-FeO-Fe_2O_3-SiO_2 system to zero CaO content. This approach was necessary because in the CaO-free system the equilibrium between slag, spinel and tridymite at fixed $P(O_2)$ is an invariant point. Direct determination of this invariant point in the CaO-free system is experimentally difficult.

2.1 General Description

The experimental procedure used in the present study is similar to that described previously by the authors.[41,42] Initial mixtures were prepared from CaO obtained from 99.0 wt pct pure $CaCO_3$ powder (calcined at 1173 K (900 °C)), SiO_2 (99.99 wt pct pure 1-3 mm fused lump that had been ground with an agate mortar and pestle), Fe_2O_3 powder (99.99 wt pct pure) and Fe powder (99.9 wt pct pure) (supplied by Alfa Aesar, Ward Hill, MA). The powder mixtures were pelletized and less than 0.3 g of sample was used in each equilibration experiment. A 10-mm × 12-mm envelope made from 0.025 mm-thick platinum foil was used to contain the sample in each experiment.

For the experiments in air atmosphere, the inner part of the reaction tube was exposed to the surrounding air

Fig. 1 (Color online) Phase diagram of the Fe-O-Si system at 1473 K (1200 °C) and P = 1 atm. Calculated with the database optimized in this study. The FSstel database[38] in the FactSage software[40] was used for the Fe-Si phases

atmosphere by opening both ends of the tube. For the experiments at fixed oxygen partial pressures between 10^{-5} and 10^{-8} atm, stream of gas with various CO/CO_2 ratios was introduced into a sealed furnace. Premixed 5 pct CO diluted in high purity Argon gas (Beta standards with ± 0.02 pct uncertainty; supplied by BOC, QLD, Australia) and high purity CO_2 (99.995 pct pure; supplied by Coregas, NSW, Australia) were used to achieve the target CO/CO_2 ratios. The proportion of gases required to achieve the target $P(O_2)$ was calculated using the FactSage software and databases.[40] The flow-rates of the gases were controlled using U-tube pressure differential type gas flowmeters. The total flow-rate of the gas inside the reaction tube was between 400 and 900 ml/min and the fluctuation of the gas flow-rate was found to be less than 1 pct of the total flow-rate.

An oxygen probe made from Y_2O_3-stabilized ZrO_2 solid electrolyte cell (SIRO$_2$®, DS-type oxygen probe; supplied by Australian Oxytrol Systems, Victoria, Australia) was used to confirm the oxygen partial pressure achieved within the furnace. The oxygen partial pressure was controlled within the accuracy of the DS-type oxygen probe, i.e. ± 0.1 $\log_{10}[P(O_2)$, atm] units.[43] A pre-calibrated working thermocouple in a re-crystallized alumina sheath was placed immediately next to the sample to monitor the actual temperature of the sample. The overall absolute temperature accuracy of the experiment was estimated to be within ± 5 K.

After the equilibration was completed, the specimen was quenched in water, dried, mounted, polished and carbon-coated. The microstructural examination and chemical compositional analysis was undertaken using EPMA (an electron probe x-ray micro-analyzer JEOL 8200L with wavelength dispersive detectors; Japan Electron Optics Ltd., Tokyo, Japan). The EPMA was operated with 15-kV accelerating voltage and 15 nA probe current. CaO, Fe_2O_3 and SiO_2 standards (supplied by Charles M. Taylor Co., Stanford, CA) were used and the Duncumb–Philibert ZAF correction software supplied with the probe was applied.

Particular attention was paid to ensure the achievement of equilibrium, as discussed previously,[41] by: (1) varying the equilibration time; (2) approaching the final equilibrium from different compositional directions and from different temperature directions; (3) analyzing the compositional homogeneity of the phases by EPMA; and (4) careful investigation of reactions specific to the system. For example, in the present study the achievement of final equilibrium of specimen at one specific condition was confirmed by two separate experiments with different initial bulk compositions, one starting from the spinel primary phase field and another from the tridymite primary phase field. The equilibrium was confirmed as both samples reached the same equilibration point.

2.2 Experimental Results

The typical appearance of the specimen backscattered electron image of a quenched slag phase, equilibrated with spinel and tridymite, is shown in Fig. 2. Energy-dispersive x-ray spectroscopy spectrums of the phases are provided in the figure. The experimental results from the present and previous studies[41,42,44] are given in Table 1. Only metal cations (Ca, Fe, Si) concentrations were measured with EPMA. Ca and Si were recalculated to CaO and SiO_2,
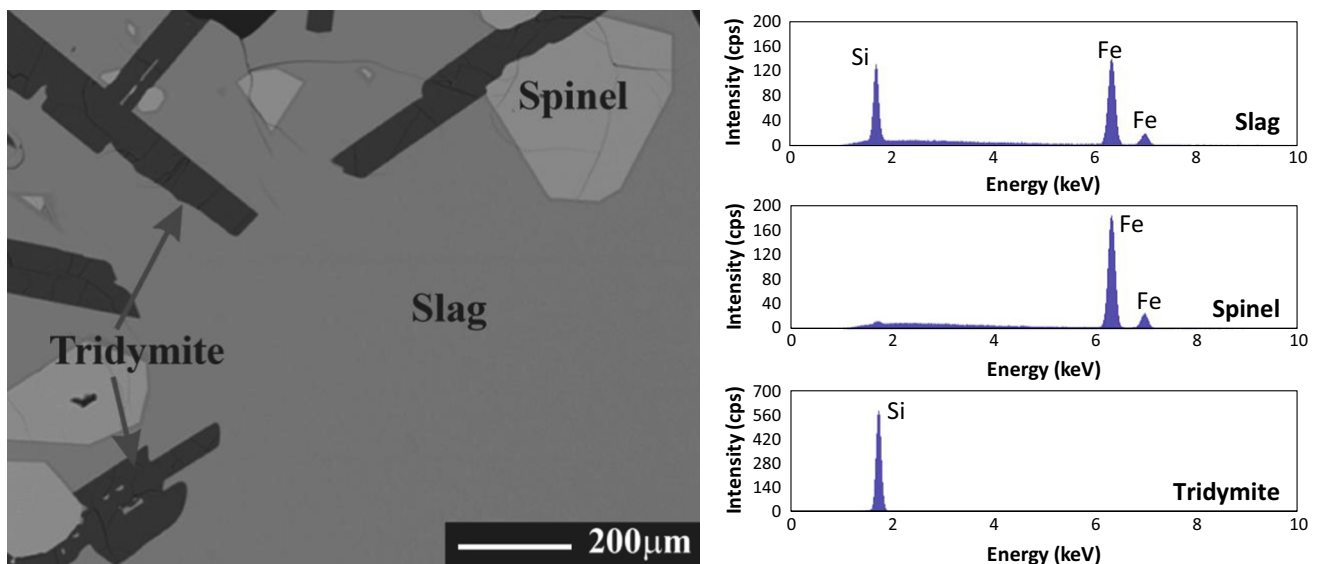

Fig. 2 (Color online) Backscattered electron image (BSE) of quenched slag in equilibrium with spinel and tridymite crystals at a fixed $P(O_2)$ in the CaO-FeO-Fe_2O_3-SiO_2 system (left hand side) and energy-dispersive x-ray spectroscopy spectrums of the phases (right hand side)

Table 1 Experimentally determined slag compositions in the CaO-FeO-Fe$_2$O$_3$-SiO$_2$ system in equilibrium with spinel and tridymite at various oxygen partial pressures and temperatures

$P(O_2)$, atm	Temperature, K, °C	Slag composition, mol pct			Molar ratio Fe/SiO$_2$	References
		SiO$_2$	"FeO"	CaO		
0.21	1673 (1400)	38.2	51.6	10.2	1.351	Present study
	1673 (1400)	37.7	51.4	10.9	1.362	Present study
	1698 (1425)	34.6	57.3	8.1	1.653	Present study
	1698 (1425)	35.6	56.7	7.7	1.590	Present study
	1738 (1465)	22.6	76.5	0.9	3.378	Present study
10^{-5}	1523 (1250)	48.5	33.1	18.4	0.682	Nikolic et al.[44]
	1523 (1250)	48.1	33.2	18.7	0.690	Hidayat et al.[41]
	1573 (1300)	43.9	45.6	10.4	1.038	Hidayat et al.[41]
	1573 (1300)	43.8	45.3	10.9	1.034	Hidayat et al.[41]
	1573 (1300)	44.2	44.5	11.3	1.008	Hidayat et al.[41]
	1593 (1320)	41.0	52.6	6.4	1.282	Present study
	1603 (1330)	40.3	54.8	4.9	1.361	Present study
	1603 (1330)	40.4	54.5	5.1	1.350	Present study
	1603 (1330)	39.3	55.9	4.9	1.422	Present study
	1618 (1345)	35.3	64.0	0.7	1.812	Present study
	1618 (1345)	35.4	63.9	0.7	1.802	Present study
10^{-6}	1473 (1200)	48.3	31.8	19.9	0.660	Nikolic et al.[44]
	1473 (1200)	48.3	31.6	20.1	0.653	Nikolic et al.[44]
	1523 (1250)	45.5	42.0	12.4	0.923	Nikolic et al.[44]
	1523 (1250)	45.4	42.0	12.5	0.925	Hidayat et al.[41]
	1523 (1250)	46.0	41.9	12.1	0.912	Hidayat et al.[41]
	1563 (1290)	39.4	56.4	4.2	1.431	Present study
	1563 (1290)	39.2	57.2	3.7	1.460	Present study
	1573 (1300)	36.4	62.2	1.4	1.709	Nikolic et al.[44]
10^{-8}	1423 (1150)	46.6	39.4	14.1	0.846	Hidayat et al.[42]
	1423 (1150)	46.6	38.7	14.7	0.831	Hidayat et al.[42]
	1463 (1190)	40.1	55.9	4.0	1.393	Present study
	1463 (1190)	40.0	56.3	3.7	1.408	Present study
	1473 (1200)	37.5	61.6	0.9	1.642	Hidayat et al.[42]
	1473 (1200)	37.8	61.4	0.8	1.623	Hidayat et al.[42]

Table 2 Temperatures and slags composition at slag–spinel–tridymite equilibrium in the FeO-Fe$_2$O$_3$-SiO$_2$ system at fixed $P(O_2)$ from extrapolation from the CaO-FeO-Fe$_2$O$_3$-SiO$_2$ system

$P(O_2)$, atm	Temperature, K, °C	Molar ratio Fe/SiO$_2$
0.21	1741 (1468)	3.876
10^{-5}	1620 (1347)	1.908
10^{-6}	1577 (1304)	1.842
10^{-8}	1476 (1213)	1.706

respectively, while all iron oxides were recalculated to FeO. This was performed for presentation purposes only, and this is equivalent to projecting the slag compositions from the oxygen-corner of the Ca-Fe-O-Si compositional space onto the CaO-FeO-SiO$_2$ ternary plane.

The temperatures and slag compositions (Fe/SiO$_2$ ratio) at the slag–spinel–tridymite equilibrium in the FeO-Fe$_2$O$_3$-SiO$_2$ system at each oxygen partial pressure given in Table 2 were obtained from extrapolation of the CaO-FeO-Fe$_2$O$_3$-SiO$_2$ data to 0 concentration of CaO in the slag as shown in Fig. 3. The information on the slag–spinel–tridymite equilibrium in the intermediate oxygen partial pressures is important since it indicates the lowest temperature at which liquid slag is stable; therefore accurate description of this equilibrium is essential.

3 Thermodynamic Models

The new optimized model parameters are reported in Table 3 for all phases in the FeO-Fe$_2$O$_3$-SiO$_2$ system including: (1) stoichiometric phases (SiO$_2$, Fe$_2$O$_3$ and
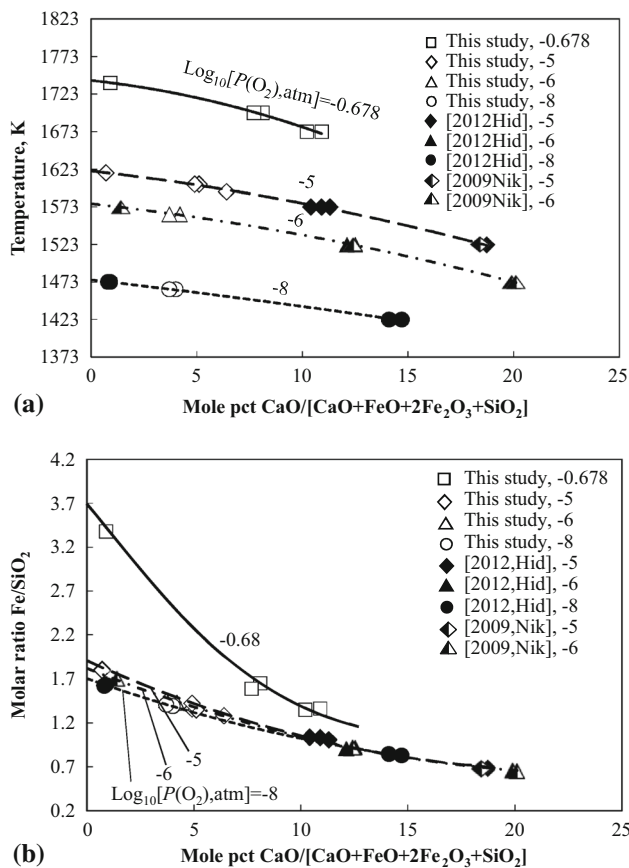
Fig. 3 Experimental results of the slag–spinel–tridymite equilibrium at various oxygen partial pressures showing: (a) temperature; and (b) Fe/SiO$_2$ ratio in slag as a function of CaO content in the slag. Symbols are experimental data[41,42,44]

Fe$_2$SiO$_4$); (2) metallic phases (fcc, bcc and liquid iron); (3) monoxide solid solution (wüstite); (4) spinel solid solution (magnetite); and (5) slag (liquid oxide FeO-FeO$_{1.5}$-SiO$_2$).

3.1 Stoichiometric Phases (SiO$_2$, Fe$_2$O$_3$ and Fe$_2$SiO$_4$)

The quartz (SiO$_2$), tridymite (SiO$_2$), cristobalite (SiO$_2$), hematite (Fe$_2$O$_3$) and fayalite (Fe$_2$SiO$_4$) solids in the FeO-Fe$_2$O$_3$-SiO$_2$ system have negligible composition variation and were described as stoichiometric phases. The thermodynamic properties for quartz, tridymite and cristobalite as reported by Eriksson and Pelton[39] and hematite as reported by Hidayat et al.[45] were adopted in the present study. Fayalite is the only stable iron-silicate compound at low pressures and the other iron-silicate compound (ferrosilite—FeSiO$_3$) is only stable at high pressures. Experimentally determined low-temperature heat capacities and the entropy,[46,47] enthalpy of formation,[48] high temperature heat content (H$_{298}$ − H$_T$)[49] and other thermodynamic data[19,21,24–29,50–52] were used for optimization of fayalite.

The heat capacity of fayalite was adopted from a previous optimization.[37] The $\Delta H°_{298}$ of fayalite was adjusted to −1478.48 kJ mol^{-1}, which is between the values from calorimetric measurements by Robie et al.[47] (−1478.17 kJ mol^{-1}) and Berman et al.[53] (−1479.36 kJ mol^{-1}). The $S°_{298}$ of fayalite was also adjusted to 150.294 J mol^{-1} K^{-1}. These changes were required to obtain a better description of heat content data by Orr[49] (Fig. 4) and oxygen partial pressures over fayalite-spinel-tridymite equilibrium as a function of temperature (see Fig. 15). Figure 4 shows comparison between experimental[49] and calculated heat content for a sample with composition of 54.5 wt pct Fe and 29.5 wt pct SiO$_2$ (the rest is oxygen). The composition is close to the theoretical stoichiometric composition of fayalite. At this composition, fayalite, spinel and tridymite are stable below the ternary eutectic temperature. Above the eutectic temperature, the portion of slag increases gradually with increasing temperature until all charge melts.

3.2 Metallic Phases (fcc, bcc and Liquid Iron)

The solubilities of oxygen in both face-centered cubic (fcc) and body-centered cubic (bcc) solid iron phases were modeled using the Bragg-Williams random mixing model:

$$g = (X_{Fe}g_{Fe}^o + X_O g_O^o) + RT(X_{Fe} \ln X_{Fe} + X_O \ln X_O) + X_{Fe}X_O L_{Fe,O}$$

(Eq 1)

where g is the molar Gibbs energy of the fcc or bcc iron; X_M is the mole fraction of element in the fcc or bcc iron; g_M^o is the molar Gibbs energy of pure elements; and $L_{Fe,O}$ is the interaction parameter between Fe and O, which is expanded as Redlich–Kister polynomial. The liquid iron solution was described using an Associate Model with Fe and O as the components. Previously optimized parameters for the solid metallic phases (fcc and bcc) by Shishin et al.[54] and the liquid metal phase by Jung et al.[38] were used in the present study.

3.3 Monoxide (Wüstite)

The wüstite in the Fe-O system was modeled in the previous assessment[45] by simple polynomial model based on the formula units shown below:

$$(1-x)FeO + xFeO_{1.5}$$

(Eq 2)

The FeO$_{1.5}$ represents the Fe^{3+} and vacancies defects resulting wüstite non-stoichiometry toward oxygen. The Gibbs energy of the wüstite is therefore given as:

$$g = (X_{FeO}g_{FeO}^o + X_{FeO_{1.5}}g_{FeO_{1.5}}^o) + RT(X_{FeO} \ln X_{FeO} + X_{FeO_{1.5}} \ln X_{FeO_{1.5}}) + X_{FeO}X_{FeO_{1.5}}L_{FeO,FeO_{1.5}}$$

(Eq 3)

482

J. Phase Equilib. Diffus. (2017) 38:477–492

Table 3 Optimized model parameters for liquid and solid phases in the $FeO-Fe_2O_3-SiO_2$ system

Compounds	Temperature range (K) or References	ΔH°_{298}, kJ mol^{-1}	S°_{298}, J mol^{-1} K^{-1}	$C_p(T)$, J mol^{-1} K^{-1}
SiO_2 (s)—Tridymite/Cristobalite	39			
Fe_2O_3 (s)	45			
Fe_2SiO_4 (s)	298-1478	−1478.482	150.294	$248.9 - 1923.8T^{-0.5} - 139.10^6T^{-3}$

Solutions	Temperature range (K) or References	Model parameters, J mol^{-1}
Fe (fcc) and Fe (bcc)	54, Bragg–Williams: (Fe, O)	
Liquid Fe	38, Associate model: (Fe, O)	
Monoxide ($Fe_{1-x}O$)—Wüs	45, Bragg–Williams: (FeO, $FeO_{1.5}$)	
Spinel (Fe_3O_4)—Sp	45,55, Compound energy formalism: $(Fe^{2+}, Fe^{3+})^{tetr}[Fe^{2+}, Fe^{3+}, Va]_2^{oct}O_4^{2-}$	
Liquid Oxide/Slag—Liq	Modified quasichemical model: FeO, $FeO_{1.5}$, SiO_2	
$Z^{Fe^{2+}}_{Fe^{2+}Fe^{2+}} = Z^{Fe^{2+}}_{Fe^{2+}Fe^{3+}} = Z^{Fe^{2+}}_{Fe^{2+}Si^{4+}} = 1.38$; $Z^{Fe^{3+}}_{Fe^{3+}Fe^{3+}} = Z^{Fe^{3+}}_{Fe^{3+}Fe^{2+}} = 2.07$; $Z^{Si^{4+}}_{Si^{4+}Si^{4+}} = Z^{Si^{4+}}_{Si^{4+}Fe^{2+}} = Z^{Si^{4+}}_{Si^{4+}Fe^{3+}} = 2.75$; $Z^{Fe^{3+}}_{Fe^{3+}Si^{4+}} = 1.38$		
$g^o_{SiO_2}$	39	
g^o_{FeO}, $g^o_{FeO_{1.5}}$, $\Delta g_{Fe^{2+}Fe^{3+}}$	66	
$\Delta g^\circ_{Fe^{2+},Si^{4+}}$		$-29{,}116.5 + 14.3T$
$q^{20}_{Fe^{2+},Si^{4+}}$		12480.9
$q^{06}_{Fe^{2+},Si^{4+}}$		$366{,}501.7 - 134.7T$
$\Delta g^\circ_{Fe^{3+},Si^{4+}}$		27213.9
$q^{01}_{Fe^{3+},Si^{4+}}$		66607.1
$q^{101}_{Fe^{2+},Si^{4+}(Fe^{3+})}$		-71270.3
$q^{012}_{Fe^{2+},Si^{4+}(Fe^{3+})}$		54392.0
$q^{021}_{Fe^{2+},Si^{4+}(Fe^{3+})}$		69454.4
$q^{201}_{Fe^{3+},Si^{4+}(Fe^{2+})}$		-62760.0
$q^{301}_{Fe^{2+},Si^{4+}(Fe^{3+})}$		91742.6

where g^o_M and X_M are the molar Gibbs energy of pure component and the mole fraction of pure component, respectively. L_{M-N} is the interaction energy parameter between two components which is expanded as polynomial in the mole fractions of the components. The optimized model parameters for wüstite from previous study by the authors[45] were adopted in the present study.
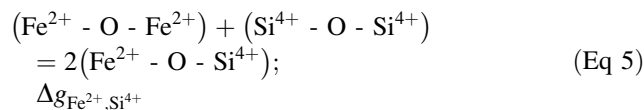
3.4 Spinel (Magnetite)

The model parameters for spinel solution from Decterov et al.[55] were used in the present study. The spinel model was developed within the framework of the compound energy formalism (CEF). The Fe^{2+} and Fe^{3+} cations were distributed between tetrahedral and octahedral sites. Neutral vacancy was introduced in the octahedral site to describe the tendency of spinel to exhibit an excess of oxygen:

$$(Fe^{2+}, Fe^{3+})^{tetr}[Fe^{2+}, Fe^{3+}, Va]_2^{oct}O_4^{2-} \qquad (Eq\ 4)$$

The Gibbs energy expression of the spinel model was explained in details in the previous study.[55]

3.5 Liquid Oxide/Slag

The liquid $FeO-FeO_{1.5}-SiO_2$ slag was modelled using the modified quasichemical model,[56–59] which takes into account the short-range ordering (SRO) of second-nearest-neighbor (SNN) cations. In the case of binary $FeO-SiO_2$ system, the SNN SRO can be expressed by the following pair exchange reaction:

$$\begin{aligned}
&(Fe^{2+} \text{ - } O \text{ - } Fe^{2+}) + (Si^{4+} \text{ - } O \text{ - } Si^{4+}) \\
&= 2(Fe^{2+} \text{ - } O \text{ - } Si^{4+}); \\
&\Delta g_{Fe^{2+},Si^{4+}}
\end{aligned} \qquad (Eq\ 5)$$

where (Fe^{2+}-O-Si^{4+}) represents a SNN pair, and $\Delta g_{Fe^{2+}Si^{4+}}$ represents the molar Gibbs energy change of the corresponding reaction. Similar pair exchange reactions can be
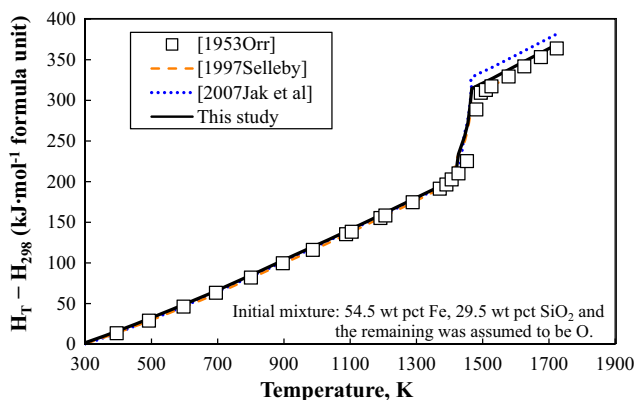
Fig. 4 (Color online) Comparison between experimental[49] and calculated heat content ($H_T - H_{298}$) of a sample with a composition of 54.5 wt pct Fe and 29.5 wt pct SiO (near theoretical composition of Fe_2SiO_4) as a function of temperature. Dashed lines are previous assessments[35,37] and symbols are experimental data[49]

applied to describe the interactions between FeO-$FeO_{1.5}$ and $FeO_{1.5}$-SiO_2 components in the melt. The overall Gibbs free energy of the slag is then given by:

$$G = \left(n_{FeO} g^o_{FeO} + n_{SiO_2} g^o_{SiO_2} \right) - T\Delta S^{config} + \left(n_{Fe^{2+}Si^{4+}}/2 \right) \Delta g_{Fe^{2+},Si^{4+}} \quad \text{(Eq 6)}$$

where ΔS^{config} is the configurational entropy of the solution, which includes the entropy of mixing given by randomly distributing the (Fe^{2+}-O-Fe^{2+}), (Si^{4+}-O-Si^{4+}) and (Fe^{2+}-O-Si^{4+}) pairs. $\Delta g_{Fe^{2+}Si^{4+}}$ can be expanded as an empirical polynomial in terms of "coordination-equivalent" fractions:[56]

$$\Delta g_{Fe^{2+},Si^{4+}} = \Delta g^o_{Fe^{2+},Si^{4+}} + \sum_{(i+j)\geq 1} q^{ij}_{Fe^{2+},Si^{4+}} Y^i_{Fe^{2+}} Y^j_{Si^{4+}}$$

$$\text{(Eq 7)}$$

where $\Delta g^o_{Fe^{2+},Si^{4+}}$ and $q^{ij}_{Fe^{2+},Si^{4+}}$ are empirical binary coefficients. $Y_{Fe^{2+}}$ and $Y_{Si^{4+}}$ are the "coordination-equivalent" fractions:

$$Y_{Fe^{2+}} = Z_{Fe^{2+}} n_{Fe^{2+}} / \left(Z_{Fe^{2+}} n_{Fe^{2+}} + Z_{Si^{4+}} n_{Si^{4+}} \right) = 1 - Y_{Si^{4+}}$$

$$\text{(Eq 8)}$$

where $Z_{Fe^{2+}}$ and $Z_{Si^{4+}}$ are the coordination numbers of Fe^{2+} and Si^{4+}, respectively. The composition of the maximum SNN SRO is determined by the coordination numbers. Improvements in the modified quasichemical model as described in the previous study[56] allow greater flexibility in setting the composition of the maximum SNN SRO based on experimental data.

The Kohler/Toop method[60] with SiO_2 treated as an "asymmetric component" was selected to extrapolate binary parameters into ternary system. Ternary parameters, $q^{ijk}_{AB(C)}$, can also be introduced to describe experimental
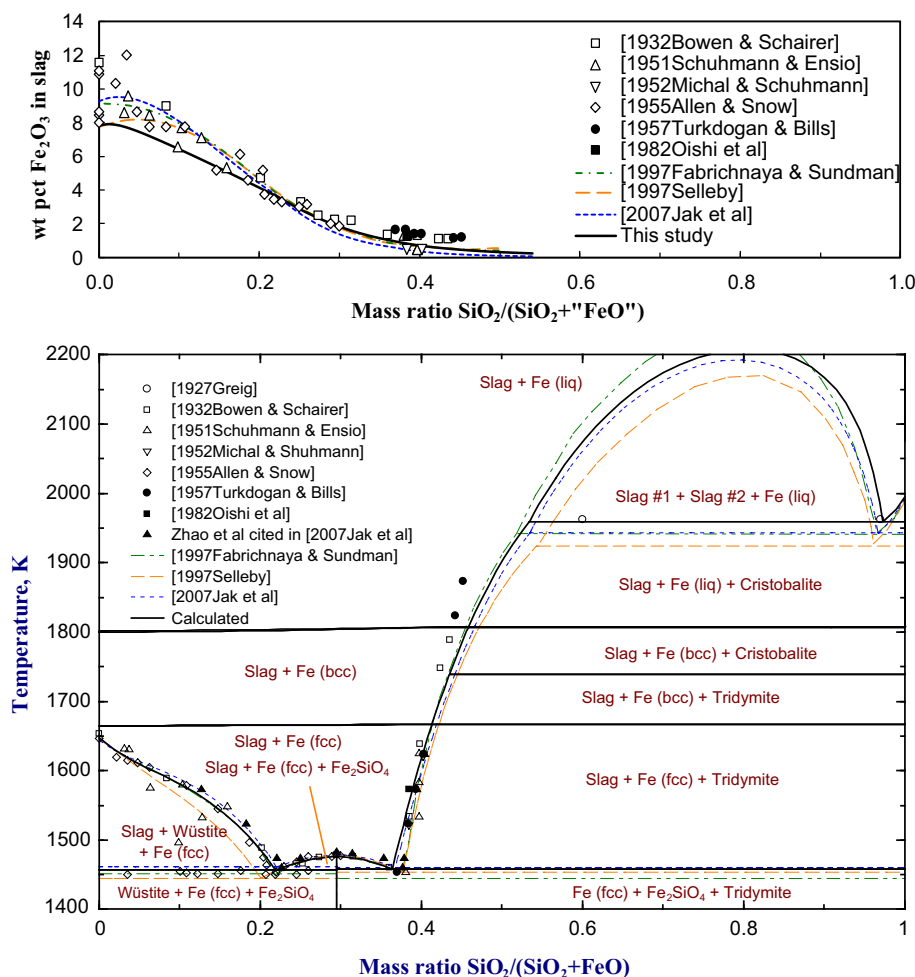
data. The $q^{ijk}_{AB(C)}$ parameters describe the effects of the third component C upon binary interactions between components A and B.[57] The optimized model parameters for the slag are given in Table 3.

4 Results and Discussion

4.1 The FeO-SiO₂ Phase Diagram in Equilibrium with Metallic Iron

The slag liquidus compositions from experimental data,[1–4,8,10,16] from previous optimizations and from the calculation using the present model parameters for the FeO-Fe_2O_3-SiO_2 system in equilibrium with metallic iron were projected onto the FeO-SiO_2 pseudo-binary plane in Fig. 5. This was done by recalculating all iron oxide in the slag to ferrous iron (FeO), i.e. composition of axis is to be interpreted as $M_{SiO_2}/[M_{SiO_2} + M_{FeO} + (M_{Fe_2O_3} \times 71.846 \times 2/159.692)]$ where M_{SiO_2}, M_{FeO}, and $M_{Fe_2O_3}$ are masses of SiO_2, FeO, and Fe_2O_3, respectively. The upper part of Fig. 5 shows the comparison of the Fe_2O_3 concentration in the slag at the liquidus between experimental data, previous and present assessments. The latest liquidus data by Zhao et al. (cited in Jak et al.[37]), obtained using an equilibration/quenching/EPMA technique was assumed to be more reliable than other data; more preference was given to this data. The calculated liquid-wüstite-fayalite eutectic temperature of 1456 K (1183 °C) is higher than that reported by Allen and Snow[4]; their work appears to be affected by the sulfur contamination in the samples. The monotectic temperature and the composition of the SiO_2-rich slag by Greig[8] at the miscibility gap are reproduced well. The composition of the FeO-rich slag reported by Greig[8] at the miscibility gap is not in agreement with the crystobalite liquidus measured by Bowen and Schairer[2] and Turkdogan and Bills,[10] and cannot be reproduced by the present and previous models.[35–37] The composition reported by Greig[8] is not the true slag liquidus composition at the monotectic temperature since FeO-rich liquid and small amount of SiO_2-rich liquid were observed in the sample. The cristobalite liquidus compositions reported by Turkdogan and Bills[10] are lower in SiO_2 compared to the calculated liquidus compositions. Turkdogan and Bills[10] estimated the liquidus compositions of cristobalite by determining the inflection points of Fe^{3+}/Fe^{2+} as function of silica which appeared when phase assemblage in samples changed from fully liquid slag to slag + cristobalite. Metallic iron inclusions were observed in some of the slags and were included in the bulk analysis of slags. The method used to determine liquidus and the presence of iron inclusions in the slag can lead to the underestimation of

Fig. 5 (Color online) "FeO"-SiO$_2$ pseudo-binary of the FeO-Fe$_2$O$_3$-SiO$_2$ system at iron saturation (bottom figure) and wt pct Fe$_2$O$_3$ in the slag along the liquidus (top figure). Dashed lines are previous assessments[35–37] and symbols are experimental data[1–4,8,10,16,37]

4.2 Slag–Metal Equilibrium

The calculated enthalpy of dissolution of tridymite in the FeO-Fe$_2$O$_3$ melts in iron crucible at 1693 K (1420 °C) is in agreement with that reported by Ban-Ya et al.[30] (Fig. 6). The optimization of the slag parameters at iron saturation was based on the enthalpy data provided by Ban-Ya et al.[30] and the phase equilibria data. The present assessment describes the enthalpy data (Fig. 6) relatively well while still providing a better description of wüstite liquidus at iron saturation (Fig. 5) compared to previous assessment by Selleby.[35] Figure 6 shows that Wu et al.[34] and Jak et al.[37] do not reproduce the enthalpy of data by Ban-Ya et al.[30]; these previous assessments appear to give more preference to phase equilibria data.

The relationships between oxygen partial pressures versus SiO$_2$/[SiO$_2$ + FeO] and Fe^{3+}/Fe$_{Total}$ in slags equilibrated with solid iron are provided in Fig. 7(a) and (b), respectively. Experimental data[3,12,17,31] are well
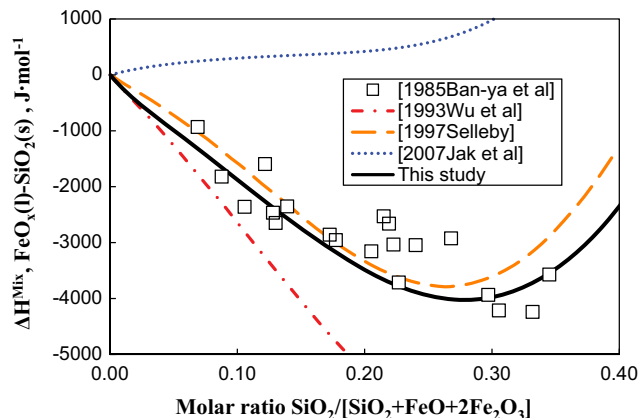
SiO$_2$ in the liquidus compositions reported by Turkdogan and Bills.[10]

Fig. 6 (Color online) Enthalpy of dissolution of tridymite in a FeO-Fe$_2$O$_3$ slag in iron crucible at 1693 K (1420 °C). Dashed lines are previous assessments[34,35,37] and symbols are experimental data[30]

reproduced by the present optimized slag model parameters. The experimental data by Kudo et al.[17] at fixed oxygen partial pressures had a higher concentration of ferric iron (Fe^{3+}) compared to others.[3,12] It is worth
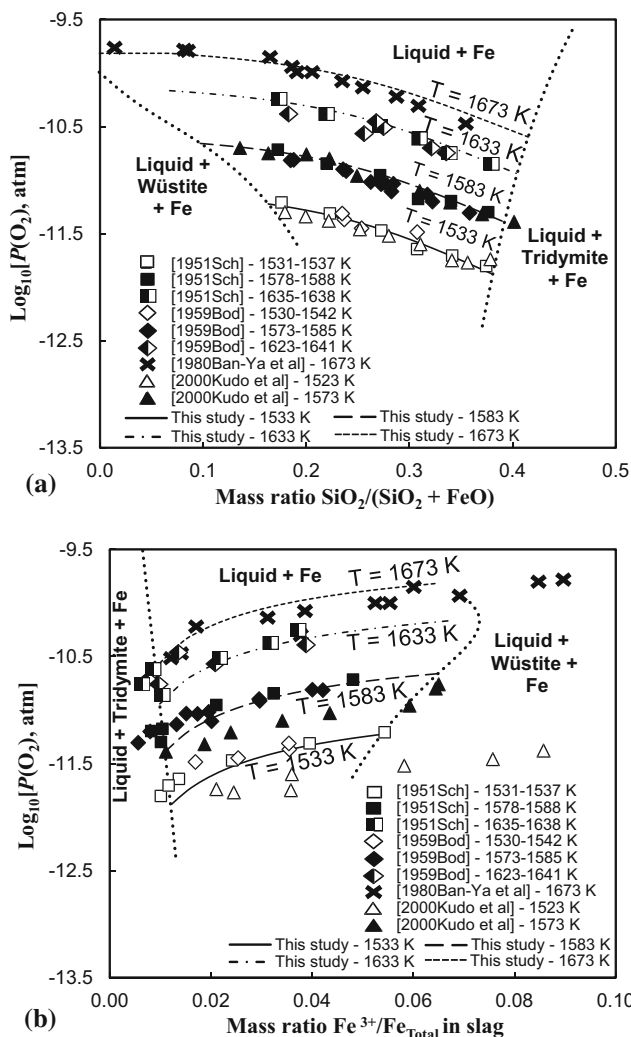
J. Phase Equilib. Diffus. (2017) 38:477–492

485

Fig. 8 Oxygen content of the metal in equilibrium with FeO-Fe_2O_3-SiO_2 slag. Symbols are experimental data[13]

Fig. 7 Equilibrium between liquid FeO-Fe_2O_3-SiO_2 slag, solid iron and gas, showing relationships between $Log_{10}[P(O_2)]$, atm vs.: (a) Mass ratio of $SiO_2/(SiO_2 + FeO)$ in the slag; and (b) Fe^{3+}/Fe_{Total} in the slag. Symbols are experimental data[3,12,15,17]

4.3 Phase Diagrams in Air and in Pure Oxygen Atmospheres

The experimental and calculated liquidus in the Fe_2O_3-SiO_2 system in equilibrium with air and pure oxygen atmospheres are compared in Fig. 9 and 10, respectively. All Fe in the slag was recalculated to Fe_2O_3. The composition of axis is to be interpreted as $M_{SiO_2}/[M_{SiO_2} + (M_{FeO} \times 159.692/(71.846 \times 2)) + M_{Fe_2O_3}]$ where M_{SiO_2}, M_{FeO}, and $M_{Fe_2O_3}$ are masses of SiO_2, FeO, and Fe_2O_3, respectively. Previous models[35–37] used only limited data.[6,7] Recent results by Liu[61] and the present experimental study (Table 2) for the system in equilibrium with air were given more weight in the present assessment. The monotectic equilibrium at the miscibility gap reported by Greig[7] is reproduced by the present model parameters (see Fig. 9).

4.4 Isothermal Sections of the FeO-Fe_2O_3-SiO_2 Phase Diagram

The isothermal sections of the FeO-Fe_2O_3-SiO_2 system determined from the calculations using the present model parameters are compared with experimental data[1,3,4,6,11,12,14–16] and with calculation results of the previous models[35–37] in Fig. 11. The data from Muan[6] suggested wider fully liquid areas at 1473 K and 1573 K (1200 and 1300 °C), conflicting with those reported by Schuhmann et al.[11] The latter study[11] was given more weight in the present assessments. Figure 12 demonstrates that the calculated oxygen isobars at fixed temperatures for the gas-slag equilibrium in the FeO-Fe_2O_3-SiO_2 system are

noting that experiment of Kudo et al.[17] was undertaken primarily to study the solubility of lead (Pb) in slag in contact with iron; the presence of PbO in their slags, although in small quantity between 0.1 and 1 wt pct, could have affected the equilibrium or analysis of their slags.

Equilibrium between slag and liquid iron at 2085 K (1785 °C), 2153 K (1880 °C) and 2233 K (1960 °C) was investigated by Distin et al.[13] using a levitation technique. The compositions of slag and liquid iron in the equilibrated samples were measured. The correlation between the oxygen content in the liquid iron and slag composition is well described by the model parameters as shown in Fig. 8.
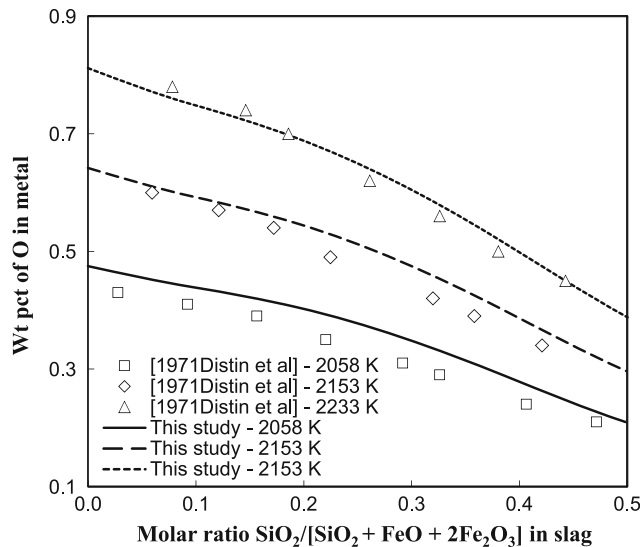
486

J. Phase Equilib. Diffus. (2017) 38:477–492

Fig. 9 (Color online) "Fe$_2$O$_3$"-SiO$_2$ pseudo-binary of the FeO-Fe$_2$O$_3$-SiO$_2$ system in equilibrium with air. Dashed lines are previous assessments[35–37] and symbols are experimental data[6,7,61]
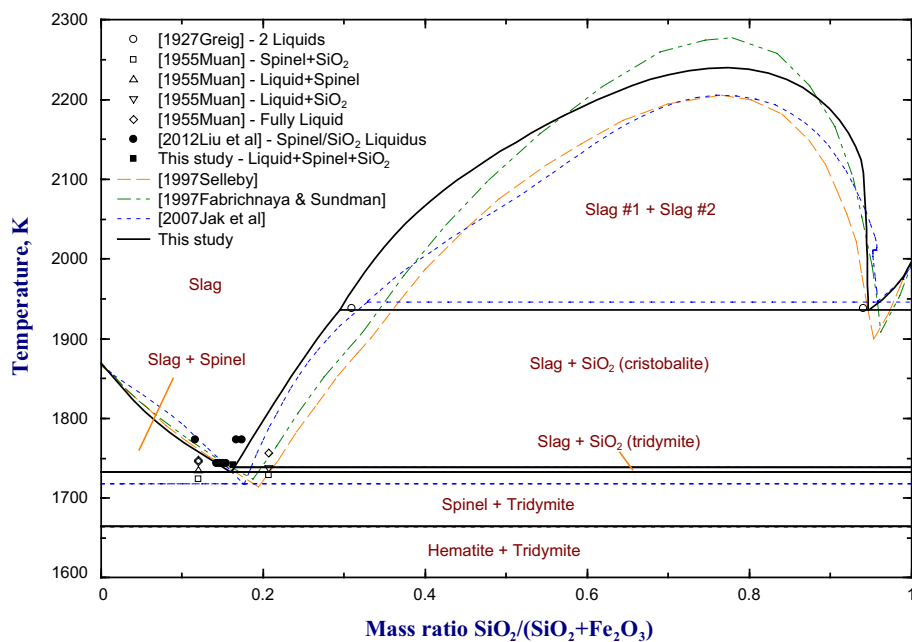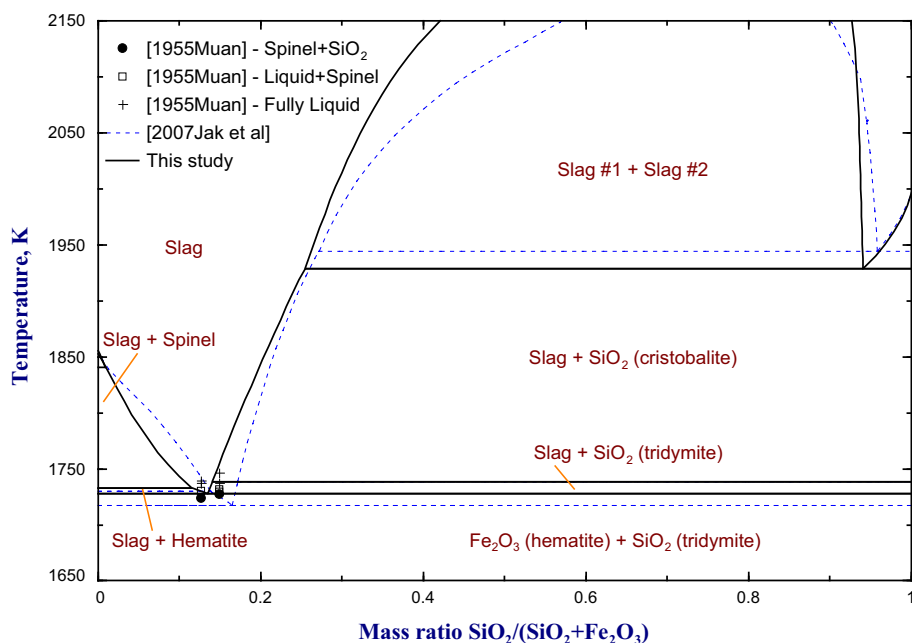

Fig. 10 (Color online) "Fe$_2$O$_3$"-SiO$_2$ pseudo-binary of the FeO-Fe$_2$O$_3$-SiO$_2$ system in equilibrium at $P(O_2) = 1$ atm. Dashed lines are from previous assessment[37] and symbols are experimental data[6]

in relatively good agreement with reported experimental data.[9,10,16] Higher Fe^{3+}/Fe^{2+} ratios in slag were reported by Muan[6] which differ from data by Oishi et al.[16] and could not be reproduced in the present assessment. It can be seen in Fig. 11 and 12 that the experimental data by Muan[6] is systematically different from the calculated values using the present model parameters. Muan[6] indicated that there were some analytical uncertainties one of which was the formation of dendritic crystals upon cooling of samples on a copper block at the bottom of the furnace. The appearance of dendritic crystals can lead to the failure

of identifying spinel/wüstite solid and to some degree can change the ratio of ferric-ferrous iron in the resulting slag.

4.5 Tridymite Liquidus

The effects of oxygen partial pressure on the Fe$_2$O$_3$ concentration and Fe/SiO$_2$ ratio along the tridymite liquidus between 1523 and 1623 K (1250 and 1350 °C) are presented in Fig. 13(a) and (b), respectively. The present model parameters give a good overall fit to the
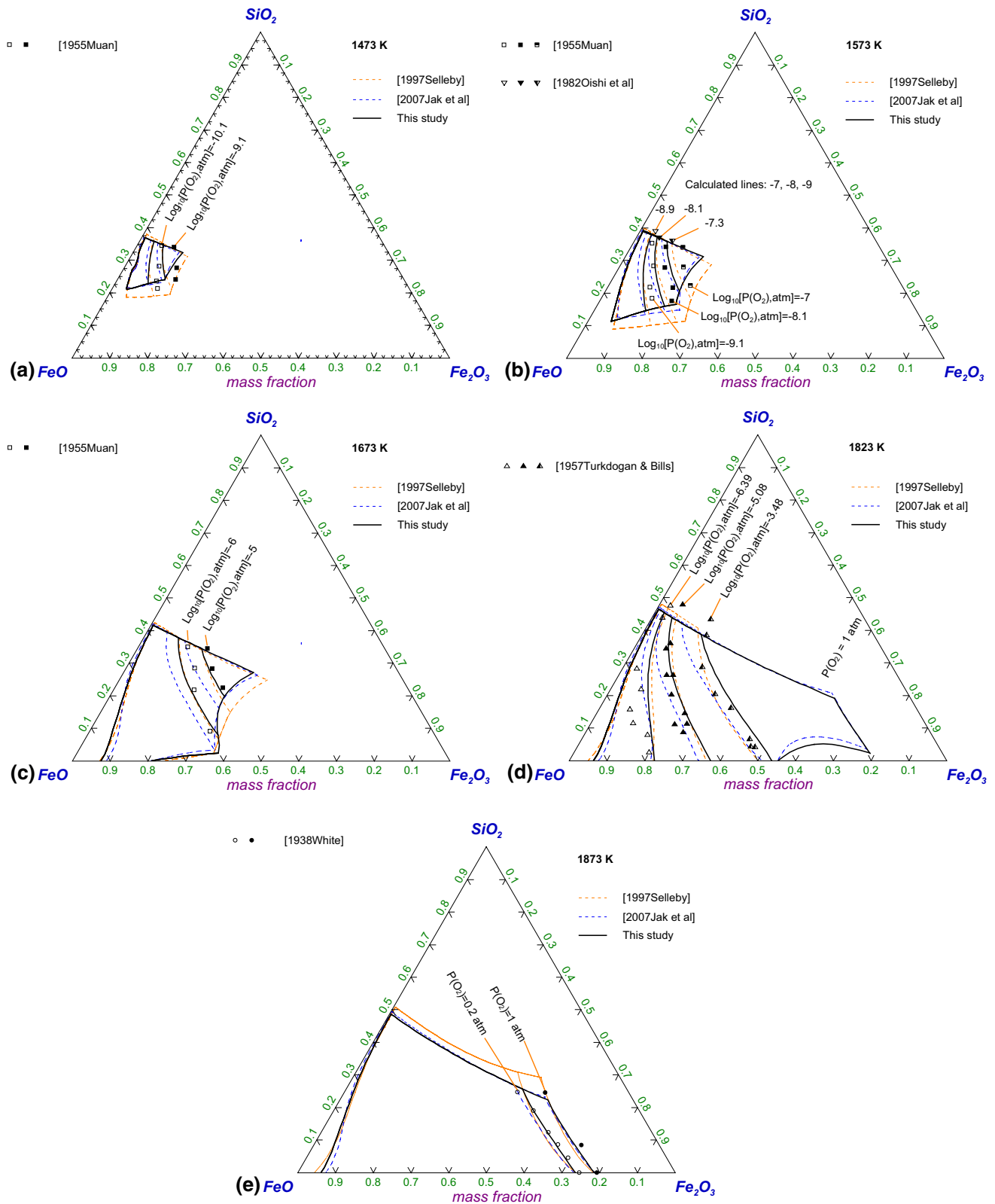
Fig. 11 (Color online) Calculated isothermal sections in the FeO-Fe$_2$O$_3$-SiO$_2$ system between 1473 and 1723 K (1200 and 1500 °C). Dashed lines are previous assessments[35–37] and symbols are experimental data[1,3,4,6,11,12,14–16]

488

J. Phase Equilib. Diffus. (2017) 38:477–492

Fig. 12 (Color online) Calculated oxygen isobars (atm) in fully liquid slag region of the FeO-Fe$_2$O$_3$-SiO$_2$ system between 1473 and 1873 K (1200 and 1600 °C). Dashed lines are previous assessments[35,37] and symbols are experimental data[6,9,10,16]

experimental data[1,6,16,41,42] over the whole range of oxygen partial pressures.

4.6 Slag–Spinel–Tridymite Equilibrium at Fixed P(O₂)

Reproducibility of the experimental slag–spinel–tridymite equilibrium at fixed $P(O_2)$ is one of important tests for the model. Figure 14 demonstrates that the present model parameters give the best fit to the experimental slag compositions at the slag–spinel–tridymite equilibrium as a function of $Log_{10}[P(O_2)$, atm] obtained in the present experimental study (Table 2) and as reported by Michal and Schuhmann.[1] Experimental data of Darken[20] and Oishi et al.[16] for the slag–spinel–tridymite equilibrium at fixed $P(O_2)$ were not included in Fig. 14 since the compositions of the resulting slags were not reported.

4.7 3-Condensed Phases Equilibria at Fixed P(O₂)

Comparison of the 3-condensed phases equilibria at fixed $P(O_2)$ between that calculated using the present model
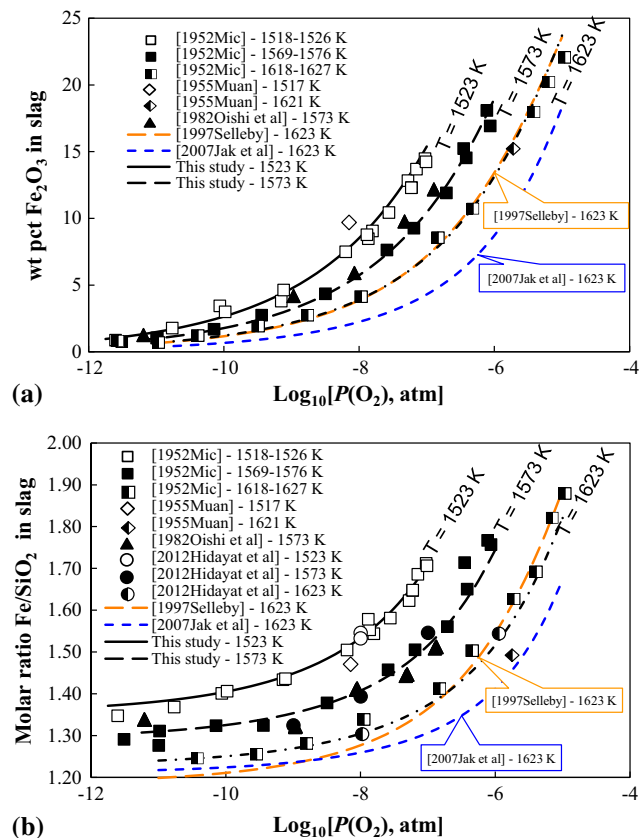

Fig. 13 (Color online) Slag-tridymite equilibrium in the FeO-Fe₂O₃-SiO₂ system between 1523 and 1623 K (1250 and 1350 °C) showing: (a) Fe₂O₃ concentration in slag; and (b) molar ratio Fe/SiO₂ in slag as a function of $Log_{10}[P(O_2)$,atm]. Dashed lines are previous assessments[35,37] and symbols are experimental data[1,6,16]

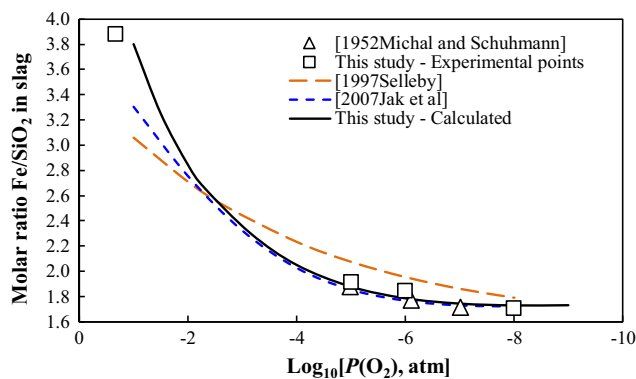**Fig. 14** (Color online) Slag–spinel–tridymite equilibrium in the FeO-Fe₂O₃-SiO₂ system showing molar ratio Fe/SiO₂ in slag as a function of $Log_{10}[P(O_2)$, atm]. Dashed lines are previous assessments[35,37] and symbols are experimental data[1]

parameters and experimental data is presented in Fig. 15 in the form of $Log_{10}[P(O_2)$, atm] versus $1/T$ (1/K) graph.[1,3,10,16,18–29] As mentioned earlier, the description of the fayalite-spinel-tridymite equilibrium in the present study has been improved compared to that of the previous assessment[37] through the adjustment of the $\Delta H°_{298}$ and $S°_{298}$ of fayalite. In addition, the slag–spinel–tridymite equilibrium at fixed $P(O_2)$ has been improved and agrees well with previous[1,16] and present experimental data (Table 2). The temperature differences for the slag–spinel–tridymite equilibrium at fixed $P(O_2)$ between the calculated values using the present model parameters and the present experimental work are within ±12 K. Discrepancy with the slag–spinel–tridymite equilibrium at fixed $P(O_2)$ is observed between the experimental data reported by Darken[20] and the calculated line. Darken[20] annealed SiO₂ rods coated with Fe₂O₃. The temperatures of the slag–spinel–tridymite equilibrium at fixed $P(O_2)$ were determined by cross-checking the temperature profile of the furnace and marks on the rods created by reaction between SiO₂ and Fe₂O₃ to form slag. The liquid slag can possibly wet the unreacted part of the SiO₂ rod leading to the underestimation of temperatures for the slag–spinel–tridymite equilibrium at fixed $P(O_2)$.

4.8 Liquidus Projection in the FeO-Fe₂O₃-SiO₂ System

The calculated univariant lines in the FeO-Fe₂O₃-SiO₂ system are given in Fig. 16. Although there are possible uncertainties in the temperature and gas composition (see section 4.4), the primary phase fields identified by Muan[6] using optical microscopy and x-ray diffraction techniques are in agreement with the present assessment. The calculated univariant line for equilibrium with metallic iron agrees with the experimental data.[1–4,10,16] The calculated

Fig. 15 (Color online) $Log_{10}[P(O_2),atm]$ vs. $1000/T$ (K) for the 3-phase equilibria in the FeO-Fe$_2$O$_3$-SiO$_2$ system. Dashed lines are previous assessments[35–37] and symbols are experimental points[1,3,10,16,18–29]
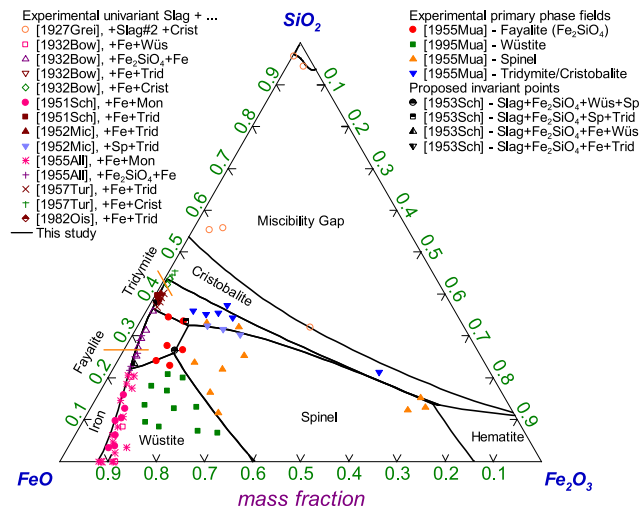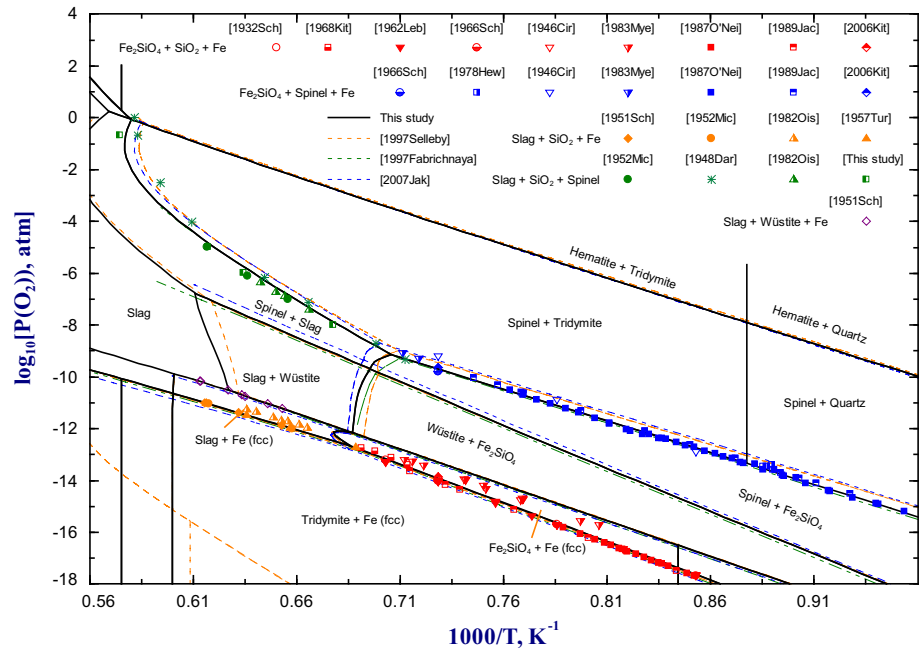

Fig. 16 (Color online) Calculated univariant lines in the FeO-Fe$_2$O$_3$-SiO$_2$ system. Symbols are experimental data[2–4,6,7,10,11,16]

invariant points agree with that reported by Schuhmann et al.[11] for the slag–fayalite–iron–wüstite, slag–fayalite–iron–tridymite, slag–fayalite–wüstite–spinel and slag–fayalite–spinel–tridymite equilibria. The calculated invariant points in the FeO-Fe$_2$O$_3$-SiO$_2$ system from present study are compared in Table 4 with previous experimental data[2,4,6,8,20] and with the previous model.[35] The calculated liquidus surface for the FeO-Fe$_2$O$_3$-SiO$_2$ system and the oxygen isobars at the liquidus temperatures are presented in Fig. 17.

The FeO-Fe$_2$O$_3$-SiO$_2$ system is the basis for many slag systems used in ferrous and non-ferrous high temperature metallurgical processes, an accurate description of the

system is therefore required. The present thermodynamic optimization has been carried out as part of the wider research program aimed at the complete characterization of phase equilibria and thermodynamic properties and the development of a thermodynamic database for the entire Al-Ca-Cu-Fe-Mg-Si-O-S multi-component system.[54,62–66] The present optimized model parameters form part of the larger database for metallic, sulfide, oxide systems, which can be used together with the FactSage software[40] for the simulation of high temperature metallurgical processes, such as sintering, steel-making, copper smelting and converting, and for the exploration or development of new processes.

5 Conclusions

A critical evaluation of phase equilibria and thermodynamic data for the FeO-Fe$_2$O$_3$-SiO$_2$ system was carried out. An experimental investigation was conducted for the slag–spinel–tridymite equilibrium in order to resolve discrepancies found in previous data. The modified quasichemical model was used to describe the Gibbs energy of the slag phase. The new model parameters reproduce a wide variety of available data within experimental error limits. Compared to the previous assessment by Selleby,[35] better agreement with the experimental data was obtained, specifically for: liquidus in wüstite primary phase field at iron saturation (Fig. 5), liquidus in tridymite primary phase field in equilibrium with air (Fig. 9), Fe/SiO$_2$ ratios in slag at reducing conditions (Fig. 13b), and slag compositions at

Table 4 Calculated invariant points involving slag in the FeO-Fe_2O_3-SiO_2 system

Reaction on cooling	Source	Temperature, K, °C		Slag, wt pct		
				SiO_2	FeO	Fe_2O_3
Slag → Fe_2SiO_4 + Spinel + Tridymite	Present model parameters	1417	(1143)	32.5	57.1	10.4
	Selleby[35]	1410	(1137)	32.2	57.0	10.8
	Muan[6]	1413	(1140)	35.0	54.0	11.0
	Darken[20] (estimated)	1391	(1118)	…	…	…
Slag → Fe_2SiO_4 + Spinel + Wüstite	Present model parameters	1438	(1165)	25.8	63.4	10.7
	Selleby[35]	1429	(1156)	22.3	64.8	12.9
	Muan[6]	…	…	22.0	64.0	14.0
	Darken[20] (estimated)	1423	(1150)	…	…	…
Slag + Fe(fcc) → Fe_2SiO_4 + Tridymite	Present model parameters	1458	(1185)	36.5	62.5	1.0
	Selleby[35]	1454	(1181)	37.7	61.6	0.7
	Bowen and Schairer[2]	1451	(1178)	38.0	60.7	1.3
Slag + Fe(fcc) → Fe_2SiO_4 + Wüstite	Present model parameters	1456	(1183)	22.1	74.3	3.6
	Selleby[35]	1444	(1171)	20.4	75.3	4.3
	Allen and Snow[4]	1450	(1177)	21.4	75.0	3.6
	Bowen and Schairer[2]	1450	(1177)	24.0	72.3	3.7
Slag → Hematite + Spinel + Tridymite	Present model parameters	1724	(1451)	13.8	15.7	70.5
	Selleby[35]	1707	(1434)	18.5	15.5	66.0
	Muan[6] (estimated)	1728	(1455)	15.0	16.0	69.0
Liquid Fe + Silica-rich slag → FeO-rich slag + Cristobalite	Present model parameters(a)	1958	(1684)	53.5	46.2	0.3
	Selleby[35](a)	1923	(1650)	54.3	45.7	…
	Greig[8](a)	1963	(1690)	58.0	42.0	…

(a) Composition of fayalite-rich liquid

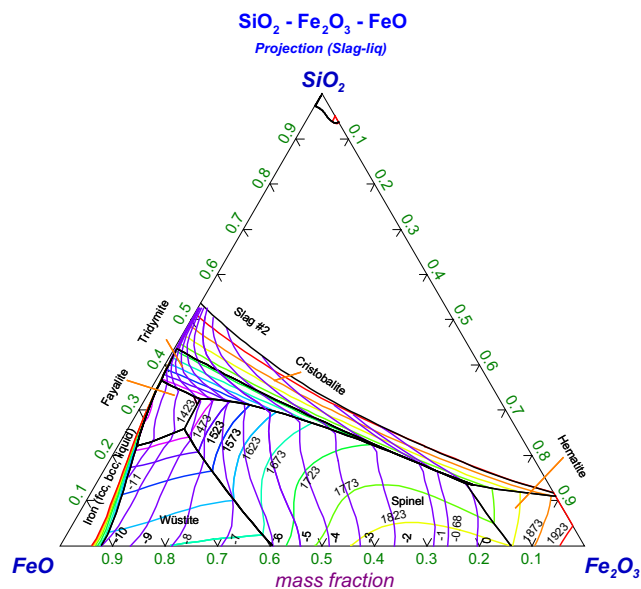**Fig. 17** (Color online) Calculated liquidus surface and oxygen isobars (Log$_{10}[P(O_2)$, atm]) at liquidus temperatures in the FeO-Fe_2O_3-SiO_2 system

the slag–spinel–tridymite equilibrium as a function of oxygen partial pressure (Fig. 14). Several improvements were introduced by the present model parameters compared to the previous model parameters by Jak et al.,[37] including: heat content of sample near fayalite composition (Fig. 4), heat of mixing in the "FeO"-SiO_2 slag at iron saturation (Fig. 6), eutectic temperatures for the "Fe_2O_3"-SiO_2 systems in air and pure oxygen atmospheres (Fig. 9, 10), and slag compositions at tridymite saturation as a function of oxygen partial pressure (Fig. 13). All of these changes are significant for the industrial applications of the database. The optimized database can be used as a basis for the simulation of various high temperature metallurgical processes, for the evaluation of possible improvement of the existing operations, or for the exploration of new processes.

492

J. Phase Equilib. Diffus. (2017) 38:477–492

References

1. E.J. Michal and R. Schuhmann, *Trans. AIME J. Met.*, 1952, **4**, p 723-728
2. N.L. Bowen and J.F. Schairer, *Am. J. Sci. (5th Ser.)*, 1932, **24**, p 177-213
3. R. Schuhmann and P.J. Ensio, *Trans. AIME J. Met.*, 1951, **3**, p 401-411
4. W.C. Allen and R.B. Snow, *J. Am. Ceram. Soc.*, 1955, **38**, p 264-280
5. B. Phillips and A. Muan, *J. Am. Ceram. Soc.*, 1959, **42**, p 413-423
6. A. Muan, *Trans. Metall. Soc. AIME*, 1955, **203**, p 965
7. J.W. Greig, *Am. J. Sci. (5th Ser.)*, 1927, **14**, p 473-484
8. J.W. Greig, *Ceram. Abstr.*, 1927, **6**(4), p 157
9. J. White, *Iron Steel Inst. Carnegie Scholarsh. Mem.*, 1938, **27**, p 1-75
10. E.T. Turkdogan and P.M. Bills, *J. Iron Steel Inst.*, 1957, **186**, p 329-339
11. R. Schuhmann, R.G. Powell, and E.J. Michal, *Trans. AIME J. Met.*, 1953, **197**, p 1097-1104
12. C. Bodsworth, *J. Iron Steel Inst.*, 1959, **193**, p 13-24
13. P.A. Distin, S.G. Whiteway, and C.R. Masson, *Can. Metall. Q.*, 1971, **10**, p 73-78
14. Y. Wanibe, Y. Yamauchi, K. Kawai, and H. Sakao, *Arch. Eisenhuttenwes*, 1973, **44**, p 711-717
15. S. Ban-Ya, A. Chiba, and A. Hikosaka, *Tetsu-to-Hagane*, 1980, **66**, p 1484-1493
16. T. Oishi, T. Goto, Y. Kayahara, K. Ono, and J. Moriyama, *Metall. Trans. B*, 1982, **13B**, p 423-427
17. M. Kudo, E. Jak, P.C. Hayes, K. Yamaguchi, and Y. Takeda, *Metall. Mater. Trans. B*, 2000, **31B**, p 15-24
18. R. Schenck, H. Franz, and A. Laymann, *Z. Anorg. Allg. Chem.*, 1932, **206**, p 129-151
19. V. Cirilli, *Gazz. Chim. Ital.*, 1946, **76**, p 331-338
20. L.S. Darken, *J. Am. Chem. Soc.*, 1948, **70**, p 2046-2053
21. B.G. Lebedev and V.A. Levitskii, *Zh. Fiz. Khim.*, 1962, **36**, p 630-632
22. R.W. Taylor and H. Schmalzried, *J. Phys. Chem.*, 1964, **68**, p 2444-2449
23. K. Schwerdtfeger and A. Muan, *Trans. AIME*, 1966, **236**, p 201-211
24. K. Kitayama and T. Katsura, *Jpn. J. Phys. Chem.*, 1968, **42**, p 525-528
25. D.A. Hewitt, *Am. J. Sci.*, 1978, **278**, p 715-724
26. J. Myers and H.P. Eugster, *Contrib. Mineral. Petrol.*, 1983, **82**, p 75-90
27. H.S.C. O'Neill, *Am. Mineral.*, 1987, **72**, p 67-75
28. K.T. Jacob, G.M. Kale, and G.N.K. Iyengar, *Metall. Trans. B*, 1989, **20B**, p 679-685
29. K. Kitayama, K. Tmahara, and T. Tamura, *Res. J. Chem. Environ.*, 2006, **10**, p 53-58
30. Ban-Ya, S., Y. Iguchi, and H. Honda: *Heat of Mixing of Liquid Fe$_t$O-SiO$_2$ Slag* in *International Symposium on Physical Chemistry Iron Steel Making*, 1982, III/39–III/44.
31. S. Ban-Ya, Y. Iguchi, H. Honda, and H. Ishizuka, *Tetsu-To-Hagane*, 1985, **71**, p 846-852
32. R.P. Goel, H.H. Kellogg, and J. Larrain, *Metall. Trans. B*, 1980, **11B**, p 107-117
33. B. Bjorkman, *Calphad*, 1985, **9**, p 271-282
34. P. Wu, G. Eriksson, A.D. Pelton, and M. Blander, *ISIJ Int.*, 1993, **33**, p 26-35
35. M. Selleby, *Metall. Trans. B*, 1997, **28B**, p 563-576
36. O.B. Fabrichnaya and B. Sundman, *Geochim. Cosmochim. Acta*, 1997, **61**, p 4539-4555
37. E. Jak, P.C. Hayes, A.D. Pelton, and S.A. Decterov, *Int. J. Mater. Res.*, 2007, **98**, p 847-854
38. I.-H. Jung, S.A. Decterov, and A.D. Pelton, *Metall. Mater. Trans. B*, 2004, **35**, p 493-507
39. G. Eriksson and A.D. Pelton, *Metall. Trans.*, 1993, **24**, p 807-816
40. C.W. Bale, E. Belisle, P. Chartrand, S.A. Decterov, G. Eriksson, K. Hack, I.-H. Jung, Y.-B. Kang, J. Melancon, A.D. Pelton, C. Robelin, and S. Petersen, *Calphad*, 2009, **33**, p 295-311
41. T. Hidayat, P.C. Hayes, and E. Jak, *Metall. Mater. Trans. B*, 2012, **43**, p 14-26
42. T. Hidayat, P.C. Hayes, and E. Jak, *Metall. Mater. Trans. B*, 2012, **43**, p 27-38
43. R.A. Mendybaev, J.R. Becket, E. Stopler, and L. Grossman, *Geochim. Cosmochim. Acta*, 1998, **62**, p 3131-3139
44. S. Nikolic, P.C. Hayes, and E. Jak, *Metall. Trans. B*, 2008, **39B**, p 179-188
45. T. Hidayat, D. Shishin, E. Jak, and S. Decterov, *Calphad*, 2015, **48**, p 131-144
46. K.K. Kelley, *J. Am. Chem. Soc.*, 1941, **63**, p 2750-2752
47. R.A. Robie, C.B. Finch, and B.S. Hemingway, *Am. Mineral.*, 1982, **67**, p 463-469
48. E.G. King, *J. Am. Chem. Soc.*, 1952, **74**, p 4446-4448
49. R.L. Orr, *J. Am. Chem. Soc.*, 1953, **75**, p 528-529
50. G. Rog and S. Kozinski, *J. Chem. Thermodyn.*, 1983, **15**, p 111-113
51. W.A. Roth and W. Bertram, *Z. Elektrochem.*, 1929, **6**, p 297-308
52. R.J. Williams, *Am. J. Sci.*, 1971, **270**, p 334-360
53. Berman, R.G., T.H. Brown, and H.J. Greenwood: *Atomic Energy of Canada Limited*, 1985, vol. TR-377, p. 62.
54. D. Shishin, E. Jak, and S.A. Decterov, *J. Phase Equilib. Diffus.*, 2015, **36**, p 224-240
55. S.A. Decterov, E. Jak, P.C. Hayes, and A.D. Pelton, *Metall. Mater. Trans. B*, 2001, **32**, p 643-657
56. A.D. Pelton, S.A. Decterov, G. Eriksson, C. Robelin, and Y. Dessureault, *Metall. Mater. Trans. B*, 2000, **31**, p 651-659
57. A.D. Pelton and P. Chartrand, *Metall. Mater. Trans. A*, 2001, **32**, p 1355-1360
58. P. Chartrand and A.D. Pelton, *Metall. Mater. Trans. A*, 2001, **32A**, p 1397-1407
59. A.D. Pelton, P. Chartrand, and G. Eriksson, *Metall. Mater. Trans. A*, 2001, **32A**, p 1409-1415
60. A.D. Pelton, *Calphad*, 2001, **25**(2), p 319-328
61. Liu, X.G.: *Experimental Phase Equilibria Studies in Oxide Systems for Copper Smelting Slags, University of Queensland, Australia, Master of Philosophy,* 2012, p. 108
62. D. Shishin and S.A. Decterov, *Calphad*, 2012, **38**, p 59-70
63. D. Shishin, T. Hidayat, E. Jak, and S. Decterov, *Calphad*, 2013, **41**, p 160-179
64. D. Shishin, E. Jak, and S.A. Decterov, *Calphad*, 2015, **50**, p 144-160
65. T. Hidayat, D. Shishin, S.A. Decterov, and E. Jak, *Metall. Trans. B*, 2016, **47**, p 256-281
66. D. Shishin, V. Prostakova, E. Jak, and S.A. Decterov, *Metall. Trans. B*, 2015, **47**, p 397-424